

# Research on Broadband High-gain Multi-beam Lens Antenna for 5G

Jianguo Jia<sup>1\*</sup>, Fangdi Mao<sup>1</sup>, Jiangbo Chen<sup>1</sup>, Yongqiang Sun<sup>2</sup>, Chenhao Zhao<sup>3</sup>, Feiyang Zhao<sup>3</sup>

<sup>1</sup>Ditai (Zhejiang) Communication Technology Co., LTD, Ningbo, China

<sup>2</sup>Ningbo Chuanyuan Precision Machinery Co., LTD, Ningbo, China

<sup>3</sup>Ningbo University of Finance & Economics, Ningbo, China

\* Corresponding author

Keywords: High-gain, Multi-beam, 5G, Plate Lomber lens antenna

Abstract: This paper designs a multi-beam antenna based on a cylindrical Lomber lens to address the shortcomings of traditional millimeter-wave high-gain antennas. The antenna uses a novel feeding scheme based on GCPW-SIW and achieves wideband, high gain and pattern stability by optimizing the electromagnetic coupling characteristics of the Vivaldi antenna. In terms of processing, based on the equivalent dielectric theory and microhole array technology, a composite dielectric structure with gradient variation of dielectric constant ( $\varepsilon_r$ =2.5-9.8) was constructed. Experimental verification shows that the scheme is engineering feasible and provides an efficient solution for phased array systems with wide frequency bands and large scanning ranges, which is of practical significance for 5G communication scenarios.

#### 1. Introduction

With the booming development of emerging fields such as smart homes, smart healthcare, smart transportation and smart cities, the Internet of Things technology has seen extensive application opportunities. As the core infrastructure of the Internet of Things, the notable features of 5th Generation Mobile Communication Technology (5G) include high information transmission rates, the ability to support a large number of users online simultaneously, and a significant reduction in latency. Become a key technology to support the efficient operation of this area [1-3]. In 5G communication systems, the antenna, as the core component for transmitting and receiving electromagnetic waves, directly affects the quality and efficiency of the entire communication link [4].

As the frequency increases, the wavelength decreases and the diffraction capability weakens. Millimeter-wave signals can even be absorbed by water vapor in the air. For stable and reliable 5G millimeter-wave communication, millimeter-wave antenna systems with high gain and low side lobes are an effective means. Under the 3GPP frequency planning, the 5G millimeter-wave band is

24.25-52.6GHz. Countries and regions further subdivide 5G millimeter-wave bands based on the allocation of their radio spectrum resources. China's 5G millimeter-wave frequency bands are expected to be defined in therange of 24.25-27.5 GHz and 37-42.5 GHz [5]. This broadband millimeter-wave antenna is conducive to covering multiple millimeter-wave frequency points and facilitating compact design and commercial application of base stations or terminal equipment. Therefore, broadband high-gain antennas applied across the entire millimeter-wave band have significant practical application value for 5G millimeter-wave communications [6].

However, millimeter-wave Massive MIMO antennas are limited in performance due to the interference between a large number of antenna units, the failure of low-frequency decoupling methods, as well as the high cost, insertion loss and noise caused by high- precision phase shifters and attenuators. In contrast, passive integrated multi-beam antennas, which cannot achieve arbitrary beam pointing, can provide fixed beam coverage in scenarios with a limited number of users and simple channel conditions, and are an important way to enhance 5G communication coverage and multi-user access capabilities [7-9]. Therefore, based on the existing learning of high-gain, low-sidelobe, wideband, multi-beam technologies and in combination with the current status of millimeter-wave technology, research on high-gain antennas suitable for 5G millimeter- wave communication is carried out [10-12].

### 2. Design and Analysis of SIW Antenna structure

Passive integrated multi-beam antennas achieve beamforming through passive components and have the advantages of low cost and low power consumption. Their structural design focuses on miniaturization and performance optimization. The mainstream schemes fall into two categories: new structures that do not require beamforming networks and classic designs based on Butler matrices.

The design of high-gain wideband multi-beam lens antennas is divided into two parts: feed and lens optimization. Since the dielectric lens is a wideband structure, the overall bandwidth of the antenna depends on the bandwidth of the feed. The Vivaldi antenna, as a broadband antenna, has the advantages of good directional radiation characteristics, wide impedance bandwidth, and simple structure, which have great practical value in the field of millimeter-wave communication technology. Because the radiation arms of the opposite Vivaldi antenna are located on either side of the dielectric substrate, the starting width of the slot line can start from zero, so the antenna can cover higher frequencies. The characteristic impedance increases as the slot width varies, thus smoothly transitioning to the characteristic impedance of free space. Therefore, the antenna has the characteristic of wide impedance bandwidth.

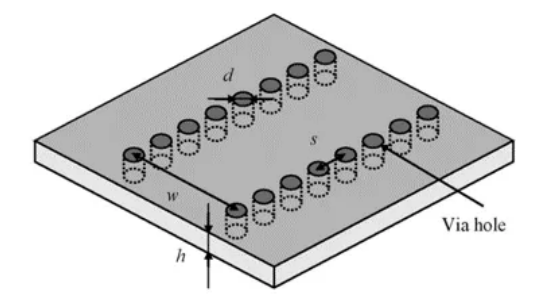


Figure 1 Basic structure of SIW

SIW transition structure the basic structure of the SIW is shown in Figure 1, and its main parameters are the diameter *Ds* of the metal through holes, the hole spacing *Ws* between two rows

of metal through holes, and the hole spacing Ss between adjacent metal through holes. Generally, Ds, Ws, and SS satisfy the following expression:

$$DS < 0.2Ig, SS \le 2DS, DS < 0.2WS \tag{1}$$

Where, Ig represents the waveguide wavelength for transmitting the main mode in the SIW structure.

The substrate integrated waveguide (SIW) uses a dielectric substrate and a metallized through-hole array to form a closed electromagnetic environment, similar to the electromagnetic confinement mechanism of a rectangular waveguide. Although this structure can effectively suppress radiative loss, it requires a transition structure to achieve impedance matching and energy coupling with the external connection. Although microband-SIW transitions are widely used in low bands, such as below the Ku band, they expose significant flaws such as high radiation loss, surface wave excitation, and increased impedance mismatch in the millimeter-wave band (>30GHz). To overcome these limitations, a ground coplanar waveguide (GCPW) -SIW structure with a gradient coupling slot transition is used, as shown in Figure 2, the electric field distribution of GCPW-SIW structure as shown in Figure 3.

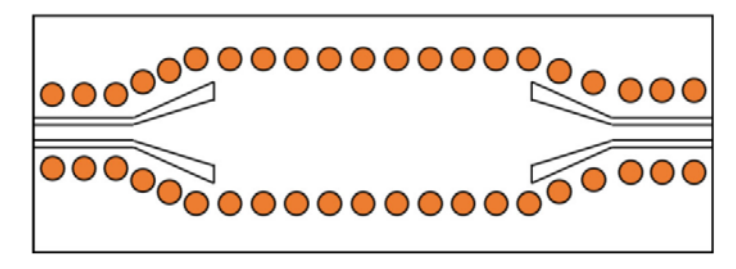


Figure 2 GCPW-SIW structure

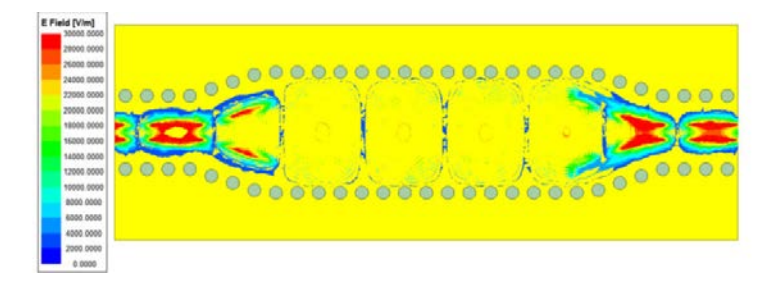


Figure 3 Electric field distribution of GCPW-SIW structure

The transition structure model is designed with a gradient coupling slot, and its core consists of an impedance adapter module and a coupling slot assembly, which can adjust the impedance while converting the electromagnetic wave propagation mode to meet the matching requirements between the substrate integrated waveguide (SIW) and the transmission line with different impedance values. The metal through-hole array symmetrically arranged on both sides of the GCPW effectively suppresses the generation of the parallel plate mode and reduces the surface wave energy loss; On the other hand, it blocks the backflow of reverse energy in the SIW, significantly improving signal transmission efficiency. This structural design achieves precise control of transmission loss and simultaneous optimization of energy efficiency through a parametric arrangement strategy.

## 3. SIW-fed Vivaldi antenna Parameter analysis

The antenna radiation section uses a GCPW-SIW feed structure, where the SIW is directly

connected to the radiation unit. Based on the electric field characteristics of the SIW perpendicular to the surface of the dielectric plate, the radiation unit selects the heel Vivaldi antenna structure for impedance matching and mode conversion, the diagram of the Vivaldi antenna structure as shown in Figure 4.

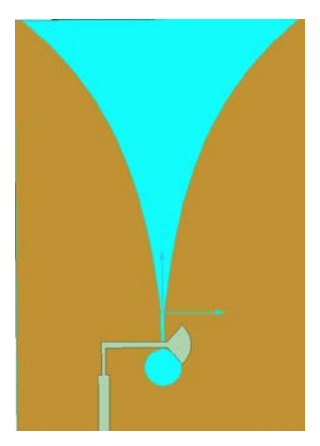


Figure 4 Diagram of the Vivaldi antenna structure

When the GCPW-SIW feed structure is directly connected to the slot line of the Vivaldi antenna, the simulation results (Figure 5) show that the antenna achieves impedance bandwidth coverage of 24-39.2GHz, but the gain characteristics vary with frequency. The red dot curve marks three significant gain minima at 28.0GHz, 32.2GHz, and 38.8GHz, reflecting the instability of radiation performance in the high-frequency band. This fluctuation may be related to the current distribution characteristics in the high-frequency radiation region of the Vivaldi antenna. During the process of high-frequency electromagnetic waves radiating and propagating in the slot line, if there is an imbalance between energy coupling and radiation matching, gain troughs are likely to form in specific frequency bands.

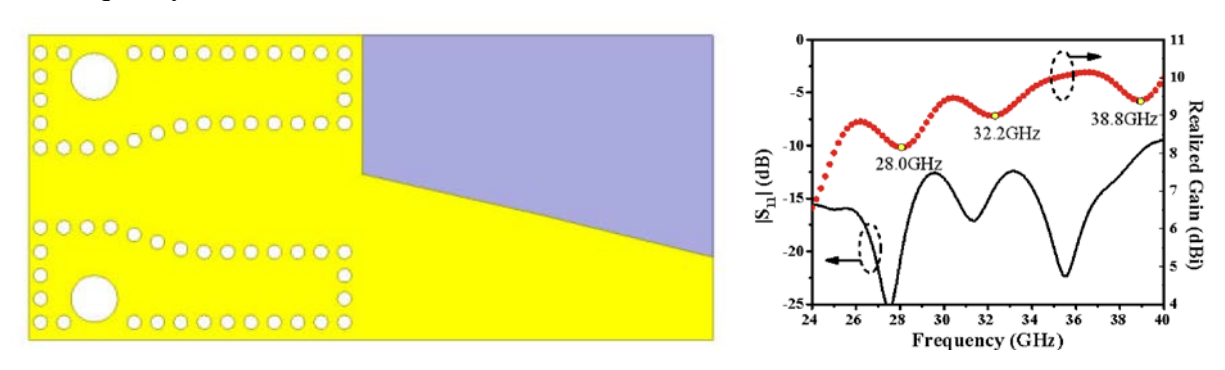


Figure 5 SIW-Vivaldi integrated structure and high-frequency characteristics performance

# 4. Analysis of Multi-beam parallel plate Lomber lens antenna

To achieve multi-beam functionality, we propose to optimize the dielectric constant distribution of the Lomber lens by gradient, precisely control its focal position, and ensure that the reverse Vivaldi antenna array is sequentially arranged in the optimized focal area to efficiently excite the multi-beam. Ultimately, a wideband multi-beam parallel plate Lombard lens antenna with both high gain and wide-angle scanning capability is achieved. One of the applications of the Lomber lens is satellite communication. Due to its good radiation characteristics, it overcomes many of the shortcomings of parabolic antennas. A single Lomber lens antenna can communicate with multiple

satellites. It is used in satellite news broadcast vehicles, mobile satellite ground stations, etc., and is currently used in many countries abroad.

The cylindrical Lomber lens antenna shown in Figure 6 has a continuous radial gradient of dielectric constant on the xoy plane, and the focal position is the generbus of the cylinder, as indicated by the red solid line. The expression of the dielectric constant is:

$$\varepsilon(r) = 2 - \frac{r^2}{R^2} = 2 - \frac{x^2 + y^2}{R^2}$$
(2)

1.8

1.9

1.0

1.0

0.0

0.2

0.4

0.6

0.8

1.0

Normalized Radius

Figure 6 Dielectric constant optimization of parallel plate cylindrical Lumber lenses

The cylindrical Lumber lens converts the cylindrical wave into a plane wave through the cylindrical symmetry structure and has one-dimensional scanning capability in the azimuth plane, with the focus originally located on the cylindrical surface, as shown in Figure 7. Because the phase center of the Vivaldi antenna deviates from the radiative surface, the dielectric constant distribution needs to be optimized so that the focus is detached from the lens surface and eventually coincides with the equivalent phase center of the feed source, thereby achieving the best convergence effect of the radiative energy. The design, while maintaining the core function of the Lomber lens, solves the traditional feed phase center offset problem through structural parameter adjustment, significantly improving the energy convergence efficiency.

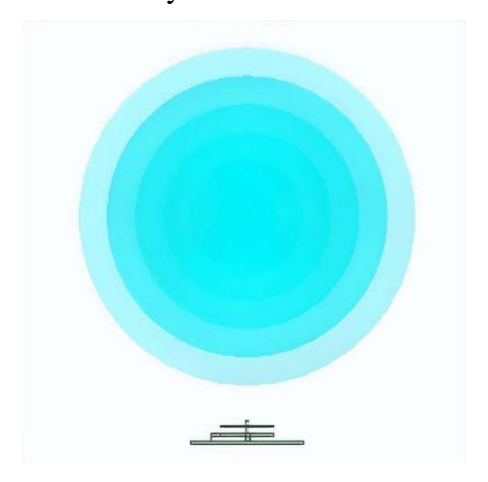


Figure 7 Schematic diagram of cylindrical Lomber lens

For a parallel plate layered Lomber lens antenna with a radius of 30mm, the number of layers is 10, and the thickness of each layer's ring is 3mm. Select a patch antenna operating at 32GHz as the feed source and perform parametric analysis on parameter F. It shows the pattern corresponding

to different focal lengths in Figure 8. It can be seen that when F < 4mm, the actual gain of the antenna increases with F, and when F > 4mm, the actual gain of the antenna decreases rapidly. Figure 9 shows the curve of the actual gain in the main radiation direction of the parallel plate layered Lomber lens antenna with respect to F. When F is greater than 12mm, the actual gain of the antenna is more than 3dB lower than the actual gain when F = 4mm, and the pattern is distorted. As the width of the flaps of the pattern widens, the side lobes increase significantly. The main cause of the pattern distortion is related to the energy overflow radiated by the feed source. When F is too large, the energy radiated by the feed source not only shines on the lens antenna but also radiates around the lens antenna. Therefore, the pattern shows higher side lobes and pattern distortion. Based on the simulation results, the value range of F is 1-6mm.

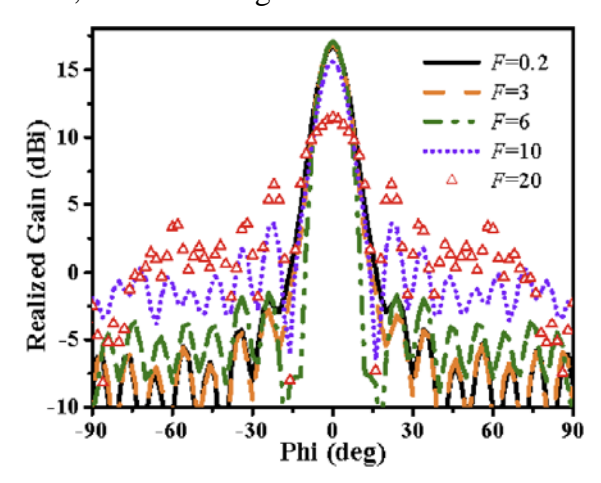


Figure 8 Orientation diagrams of the xoy planes corresponding to different focal lengths

We refer to the analysis of the electric field distribution on the surface. The black arrows in the figure indicate the direction of the electric field vector, and it is observed that the end of the electric field vector shows a linear oscillation trajectory along the z-axis over time. This feature indicates that the vibration direction of the electric field vector in the parallel plate lens is always consistent with the plane formed by the propagation direction (z-axis), and thus it is determined that the polarization mode along the propagation direction is vertical polarization.

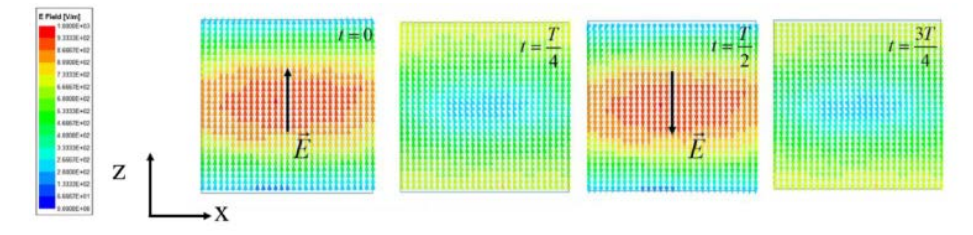


Figure 9 Electric field distribution on the reference plane at 33GHz

## 5. Antenna processing and testing

The Lomber lens antenna is manufactured by a special design method using Rogers 5880 boards with a dielectric constant of 2.2 as the substrate and a gradient dielectric constant structure processed through PCB punching. The actual machined part, designed to be 10mm thick, with a total thickness of 9.958mm. The accompanying 70mm diameter brass parallel plate is 5.3mm thick, machined and tightly connected to the lens with nylon screws, which ensures structural stability and reduces air layer interference, resulting in an overall thickness of 20.5mm, as shown in Figure 10.



Figure 10 Physical view of the parallel plate lens antenna



Figure 11 Physical view of the feed antenna

Figure 11 shows a physical image of the feed antenna, which is based on Rogers 5880 plates and has a thickness of 0.381mm. The wire width at the feed position is only 0.7mm, so a solder-free connector is used to feed the feed antenna.

Figure 12 shows the pattern test results of the feed antenna at different frequency bands. The E-plane pattern (red curve) is overall consistent with the simulation data, but at 38GHz, due to significant fluctuations in the test signal, there is a 14° deviation between the measured and simulated values of the half-power lobe width of the E-plane in this frequency band. In contrast, the H-plane pattern (blue curve) shows obvious band differences: pattern distortion occurs in the low band (26GHz/30GHz), while the test results in the high band (35GHz/38GHz) tend to be consistent with the simulation curve. This difference in band characteristics may be related to variations in the electromagnetic field distribution of the antenna structure at different wavelengths. Overall, the antenna could serve as a feed source for a lens antenna for multi-beam requirements.

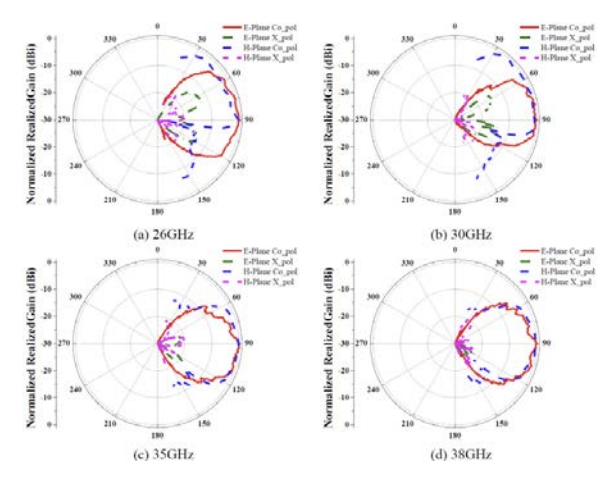


Figure 12 Pattern of the feed antenna at different frequency bands

#### 6. Conclusions

This study focuses on the innovative design of key technologies for linearly polarized feed systems. At the feed structure level, a novel feed scheme based on GCPW-SIW was proposed. By optimizing the electromagnetic coupling characteristics of the second-to-back Vivaldi antenna, a comprehensive performance breakthrough of wideband, high amplification and pattern stability was successfully achieved. In terms of the implementation path, based on the equivalent medium theory, a microhole array processing method was proposed. By controlling the aperture size and arrangement density, a composite dielectric structure with dielectric constant gradient variation ( $\epsilon r=2.5-9.8$ ) was successfully constructed. The engineering feasibility of the scheme was verified by experimental tests. The design breakthrough provides a new solution for phased array systems with wide frequency bands and large scanning ranges.

# **Funding**

This work was supported by the financial support from the District Key Project in High-Tech district of Ningbo [grant number 2024CX050002], projects of major scientific and technological research of Ningbo City (2022Z090(2022Z050), 2023Z050(the second batch)), projects of major scientific and technological research of Beilun District, Ningbo City(2022G009), projects of scientific and technological research of colleges student's of China (202313022036, 202413001008).

#### Reference

- [1] Jiang Z H, Gregory M D, Werner D H. Broadband High Directivity Multibeam Emission Through Transformation Optics-Enabled Metamaterial Lenses. IEEE Transactions on Antennas & Propagation, 2012, 60(11):5063-5074.
- [2] Zhihao, Jiang, D. G. Micah, and H. W. Douglas. Broadband High Directivity Multi-Beam Emission Through Transformation Optics Enabled Metamaterial Lenses. IEEE Transactions on Antennas & Propagation, 2012.
- [3] Yin, Si Yu, et al. Fan-Shaped Multibeam Metasurface Lens Antenna for High Crossover Levels and Stable Radiation Gain. IEEE antennas and wireless propagation letters 2024, (6):23.
- [4] Abdelaziz, A. H., et al. Reducing radar cross section through absorption metamaterial antenna for concealment and detection applications. AEU: Archiv fur Elektronik und Ubertragungstechnik: Electronic and Communication, (2024):178.
- [5] Xue, D. H., et al. Characteristics of serpentine circular groove waveguide slow-wave structure. High Power Laser and Particle Beams, 2006, 18 (9):1535-1538.
- [6] Manikandan, B., et al. High gain hybrid composite of DRA for 5G millimeter wave application. AIP Conference Proceedings, 2023, (1):7.
- [7] Denidni, Tayeb A, and E. T. Libar. Wide band four-port butler matrix for switched multibeam antenna arrays. Personal, Indoor & Mobile Radio Communications, Pimrc IEEE on IEEE, 2003.
- [8] Shen, Yaokun Shi Zhe. Wide-field large-angle beam splitters based on polarization-insensitive coding metasurfaces. Journal of the Optical Society of America, A: Optics, Image Science and Vision, 2024,41 (12):6.
- [9] T.S. Rappaport, Y. Xing, G.R. MacCartney, A.F. Molisch, E. Mellios, J. Zhang, Overview of Millimeter Wave Communications for Fifth-Generation (5G) Wireless Networks With a Focus on Propagation Models. IEEE Transactions on Antennas and Propagation, 2017, 65(12): 6213-6230.

- [10]Y. Niu, Y. Li, D. Jin, L. Su, A.V. Vasilakos, A survey of millimeter wave communications (mmWave) for 5G: opportunities and challenges. Wireless Networks, 2015,21(8): 2657-2676.
- [11] Lakshman, Praveen Haandi, et al. High-gain circularly polarized metasurface antenna for NR257 band millimeter-wave 5G communication. Indonesian Journal of Electrical Engineering & Computer Science 2025,37 (2).
- [12]Ye J, Li T, Han M, et al. Metasurface-Inspired Wideband Circularly Polarized Antenna Array in Ka-Band Using Characteristic Mode Analysis. IEEE Antennas and Wireless Propagation Letters, 2024, 23 (1) 389-393.